Time-resolving x-ray diagnostics for ICF (invited)

P. A. Jaanimagi, D. K. Bradley, J. Duff, G. G. Gregory,[a] and M. C. Richardson

Laboratory for Laser Energetics, University of Rochester, 250 East River Road, Rochester, New York 14623-1299

(Presented on 17 March 1988)

X-ray streak cameras, which can be coupled to a large variety of spectroscopic or imaging devices, provide an important research tool for studying laser fusion plasmas. Generally, several of these instruments are deployed simultaneously on a given experiment to furnish a comprehensive data set of the x-ray emission spectrum and target hydrodynamics. Of particular importance is the ability to do quantitative analysis with the data set. This allows meaningful comparisons to be made with simulations. The sophistication of the hydrodynamic and atomic physics codes is such that qualitative analysis is insufficient. Various simple parameters in these codes are benchmarked against experimental measurements before more detailed calculations are performed. As in all diagnostic systems the range of linear response must be well defined. In this article we will discuss some of the constraints inherent in streak camera systems and how they affect the acquisition and analysis of the experimental results. Examples illustrating our current capabilities for diagnosing experiments on the OMEGA laser fusion facility will be presented.

INTRODUCTION

Time-resolving x-ray instrumentation constitutes a major subset of the extensive array of diagnostics used to investigate ICF plasmas. These intruments include x-ray diode (XRD)[1] or photoconductive detector (PCD)[2] based single-channel spectrometers recorded with an oscilloscope; two-dimensional x-ray imaging and spectroscopy with framing cameras incorporating microchannel plate (MCP) technology[3]; and x-ray streak cameras coupled to various imaging or spectroscopic devices.[4] The 2-D formats are recorded either on film or electronically with CCD arrays. In simple terms the challenge for these diagnostics is to measure the absolute x-ray flux emitted from the target with 1-ps time resolution, while either imaging the emission with 1-μm spatial resolution or recording the spectrum with a resolution E/dE of 1000 or more. In addition, this is to be measured with a linear dynamic range of three orders of magnitude, in various spectral bands ranging from 10 eV to 100 keV. Clearly this exceeds the capabilities of current technologies, and in this article we will examine some of the limitations of the instruments, focusing primarily on streak cameras.

First, consider our ability to make quantitative measurements with the diagnostics. This is of particular importance as it allows meaningful comparisons to be made with the predictions of hydrodynamic and atomic physics codes modeling the experiments. Generally the input parameters for the simulations are well known. For example, the laser energy delivered to the target can be measured to 1% accuracy, the laser pulse shape (600-ps FWHM Gaussian) can be diagnosed with a 25-ps time resolution optical streak camera, and the target wall thickness is measured interferometrically to a fraction of a wave. The sophistication of the codes is such that if on OMEGA experiments the predicted implosion time differs from the experimentally measured value by more than 50 ps, an error was most likely made in determining the laser or target parameters.

The calibration of the diagnostics must be performed very carefully. Then, cross correlating between instruments further increases confidence in our measurements. Since XRDs, PCDs, and streak cameras are sensitive to optical or UV radiation, and short pulse sources are readily available, the calibration of the time axis on these devices is straightforward. One simply uses an étalon of known spacing to generate a train of short optical or UV pulses separated by a fixed time delay. A time axis calibration accuracy of better than 5% can be made routinely with this technique.

The absolute calibration of the recording sensitivity of a device is much more difficult and it depends strongly on the stability of its response function over long periods of time. XRDs with simple metal cathodes have been shown to be stable for several months, even with frequent vacuum cycling and occasional exposure to air. Typically the XRD photocathode response is measured at a series of discrete energies with monochromatic x-ray sources, and theoretical curves for the photoelectric quantum efficiency are normalized to these points. The accuracy of the calibrated XRD response to a broadband source then depends on how well we know its spectrum. Generally an array of four or more XRDs, separately filtered for different spectral response, is used to measure the total x-ray fluence to $<5\%$ accuracy. PCDs have also been successfully calibrated. In addition, they have a flat spectral response, and are more sensitive per unit area than XRDs, especially at higher x-ray energies.

The two-dimensional format of framing and streak cameras makes the task of calibrating these instruments much

 0034-6748/88/081854-06$01.30

more complex. Further, unless they are fabricated as vacuum-sealed units, they appear to be much less stable than XRDs or PCDs. Problems arise with windowless, gated MCP devices due to the sensitivity of the MCP gain to the residual background gas pressure in the individual channels. In addition, since the MCP gain is approximately proportional to the tenth power of the applied voltage, the stability of the driving electronics becomes a major issue. Exceptional voltage stability is also a prerequisite for reproducibility of the optical gain in the MCP-based image intensifiers that are used in most streak cameras. X-ray streak cameras also have problems with the stability of the photocathode response; CsI is hydroscopic and thin Au photocathodes deteriorate due to the migration of the Au ions under the strong electric fields at the cathode. The best reported absolute calibration of an x-ray streak camera is to an accuracy of 30% by Kauffman *et al.*,[5] on a three-channel, broadband (x-ray mirror and filter) spectrometer, carefully cross correlated against a set of spectrally matched XRDs.

Even though x-ray streak cameras are extremely difficult to calibrate absolutely, they do offer many advantages. The availability of a few hundred resolution elements along the photocathode length gives these devices the very large information capacity needed for time-resolved x-ray imaging or spectroscopy. Streak cameras have time resolutions better than 10 ps and the sensitivity to detect single photoelectrons. The linear dynamic range of these instruments approaches two orders of magnitude, and they can be configured for useful sensitivity over the full spectral range of 10 eV to 100 keV.

At the OMEGA laser facility we have five x-ray streak cameras; one is used for time-resolved imaging, the others for x-ray spectroscopy.[6] All of the cameras that are coupled to spectrographs use the same large-format streak tube design.[7] The photocathode slit measures 1×45 mm. The 1-mm-wide slit provides enhanced sensitivity yet is demagnified to $\sim150\ \mu$m by the electron optics so that it does not degrade the time resolution. The long slit allows large spectral ranges to be diagnosed on a single shot as well as providing room for locating the optical timing fiducial channel.

In the following sections of this article we will discuss some of the limitations of current x-ray streak camera technology; examine the time-resolved x-ray imaging instrumentation at LLE; and describe a new reflection mode photocathode x-ray streak camera for VUV and soft-x-ray spectroscopy.

I. X-RAY STREAK CAMERAS

X-ray streak cameras are basically demountable versions of their optical counterparts, and many aspects of their characterization are identical. The main difference is that x-ray photocathodes are based on the emission of secondary electrons that have a much larger initial energy spread than the primary photoelectrons produced in visible-light-sensitive photocathodes. This has a deleterious effect on both the temporal and spatial resolution of the x-ray streak camera.

Time-of-flight dispersion (Δt) due to the finite spread in the initial photoelectron energies (ϵ) is the primary limiting factor in the time resolution capabilities of all streak cameras. Generally, for optical cameras one only needs to consider the dispersion in the initial acceleration region, neglecting the contributions through the focusing, final accelerating, and drift regions. However, for x-ray streak tubes these other components can significantly increase Δt. Simple formulas to estimate properly the time-of-flight dispersion can be derived if one approximates the axial potential in the streak tube as in Fig. 1. Using simple nonrelativistic, constant-acceleration formulas for the motion of an electron in a planar diode or a drift region, one can easily calculate the transit-time difference in each successive region for electrons with initial axial velocities corresponding to energies of zero and ϵ. For example, the electrons enter section two with initial energies of V_1 and $V_2+\epsilon$. The time-of-flight dispersion in each region to order ϵ can be written as

$$\Delta t_1 = kd_1V_1^{-1}(\epsilon^{1/2} - \epsilon V^{-1/2}/2)\,,$$
$$\Delta t_2 = kd_2V_1^{-3/2}\epsilon/4\,,$$
$$\Delta t_3 = kd_3(V_2 - V_1)^{-1}\epsilon(V_1^{-1/2} - V_2^{-1/2})/2\,,$$
$$\Delta t_4 = kd_4V_2^{-3/2}\epsilon/4\,,$$

where $k=(2m/e)^{1/2}$. The sum of all these contributions provides a more realistic estimate of the time resolution of the streak tube.

The large-format x-ray streak tube used at LLE has a calculated time-of-flight dispersion $\Delta t = 1.6\epsilon^{1/2} + 0.7\epsilon$, with Δt in ps and ϵ in eV. When combined with the 2-eV secondary electron energy distribution for CsI from Ref. 8, this tube can achieve a time resolution of 3–4 ps. Consider the same tube with an S-20 photocathode, illuminated with 800-nm light, at the long-wavelength cutoff of the cathode sensitivity. This would result in an initial photoelectron energy spread of <0.1 eV, yielding a time-of-flight dispersion of less than 1 ps.

All of the standard crossover-type x-ray streak tubes operate with a time resolution in the 4–20-ps range, and do not seem able to break the 1-ps barrier. However, there is one streak tube design that appears to be capable of subpicosecond time resolution with an x-ray photocathode. This is the proximity-focused streak tube designed by Lieber.[9] This tube has an accelerating field of 7 kV across the 1-mm gap between the photocathode and the passive MCP collimator, followed by a 25-mm drift region to the phosphor. The calculated time-of-flight dispersion is less than 1 ps for a 3-eV

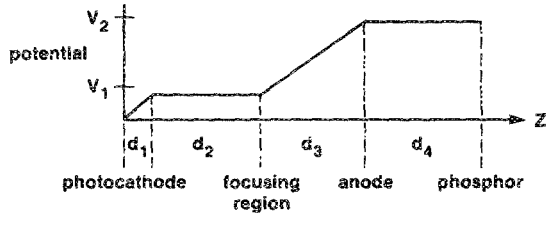

FIG. 1. Approximate axial potential distribution for a standard crossover-type streak tube. d_1 is the initial accelerating region, d_2 is the focusing region, d_3 is the final accelerating region, and d_4 is the drift zone to the phosphor screen. V_1 is the accelerating potential and V_2 is the anode potential.

initial electron energy. Given the relatively poor spatial resolution (250 μm) and a deflection sensitivity of 2 kV/cm, one requires a 5 kV per 100 ps voltage transient to drive the tube. However, such a large voltage transient is readily available from laser-driven semiconductor switches.[10]

The large initial energy spread of the secondary electrons emitted from x-ray photocathodes also degrades the spatial resolution of the devices; this is equivalent to chromatic aberration in light optics. Further problems arise due to field curvature for nonparaxial trajectories; this is most apparent in large-format streak tubes. However, the limiting component in most streak cameras is the image intensifier. The characterization of spatial resolution is usually given in terms of the contrast transfer function (CTF), defined as

$$\mathrm{CTF} = (I_{\max} - I_{\min})/(I_{\max} + I_{\min}) .$$

We have measured a CTF of 25% at 10 lp/mm for the commonly used ITT F4113 proximity-focused MCP intensifier (full curves can be found in Ref. 11). A practical rule of thumb for unambiguously resolving features is to require a CTF > 50%, which in this case requires designing for 5 lp/mm going into the image intensifier. Since the signal from the streak camera phosphor that is presented to the image intensifier will not have 100% modulation, the system CTF will be < 50%. One must also consider how many pixels in the temporal direction must be averaged to obtain the desired CTF.

For applications where one requires a large dynamic range, a different problem is encountered as illustrated by the line spread function of the ITT F4113 image intensifier in Fig. 2. For this measurement a 100-μm-wide slit, cut in a 100-μm-thick metal foil, was contacted to the fiber-optic faceplate of the intensifier and illuminated with a noncollimated light source. The film density was corrected to intensity using a carefully constructed D–log E curve. Two different components of flare can be seen in this figure. The first has a peak at the 1.3% level and a FWHM of 0.4 mm, and the second component has a peak at the 0.03% level and a radius of 2.0 mm. A few possible sources for the flare include photon scattering and lateral transmission in the 6-mm-thick fiber-optic faceplate, fluorescence generated by photoelectrons hitting the webbing at the MCP input and feeding back to the photocathode, and poor end spoiling of the MCP output. We are currently investigating these and other possibilities.

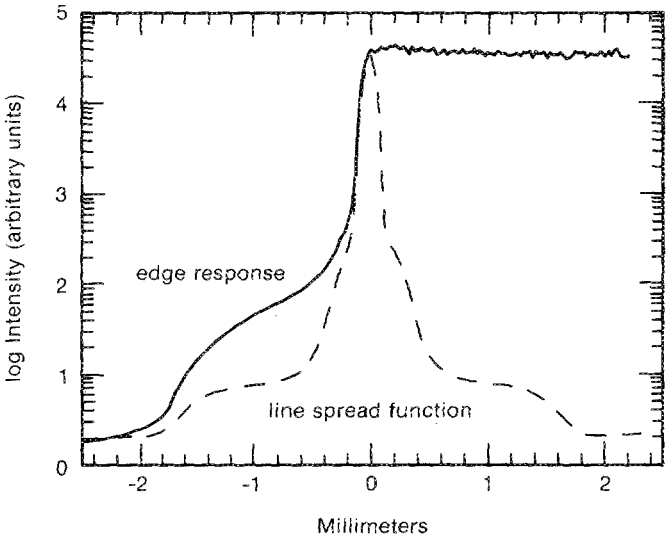

FIG. 2. Line spread function (dashed curve) of the ITT F4113 image intensifier illuminated through a 100-μm-slit in contact with the fiber-optic input faceplate, and edge response function (solid curve) for the same image intensifier.

The edge response of the same intensifier is also presented in Fig. 2, and in this case the flare becomes significant at the 5% level. These curves clearly demonstrate that the fidelity of recording sharp exposure gradients is severely restricted by the image intensifier response. It is important to realize that one can lose the fidelity of recording pulse shapes even if the input-to-output transfer characteristics of the device remain linear over 4–5 orders of magnitude. This is because the transfer function just measures either the peak height or the area under the curve.

Another aspect of the fidelity of the streak camera records is the uniformity of the response to a constant input flux over the full spatial extent of the image.[12] Characterization of the system flat field response is a prerequisite for quantitative analysis of the streak data, as the overall system gain can easily vary by factors of 2 across the image. Spatially nonuniform gain in an image intensifier is demonstrated by the gentle slope on the illuminated section of the edge response curve in Fig. 2. Manufacturer's specifications on intensifier gain nonuniformity may be as high as 40%.[13] Other sources of spatial nonuniformity include variations in the photocathode quantum efficiency, phosphor conversion efficiency, the transmission of any coupling optics, and vignetting in the electron optics. In addition, geometric distortions and streak speed nonlinearities will also contribute to apparent variations in the system response.

The precision or the signal-to-noise ratio of the measurements we make with the diagnostics is also important. Given the statistical nature of the streak images, consider that for a dynamic range of 1000 we need to record 10^6 photoelectrons per time and spatial resolution element. This assumes that there is no noise in the system. Set the time resolution to 1 ps, and the spatial resolution element at the streak tube phosphor to 200 μm square, to match the intensifier resolution. The corresponding area at the cathode for the LLE large-format streak tube is 1 mm $\times$ 200 μm with a resultant photoelectron current density of 80 A/cm^2. This is four times greater than the space-charge-limited current density in the cathode region of this tube. Only if we give up the concept of resolution elements, and consider the photocathode length to be divided into $\sim$1-cm-wide channels, can we even conceive of attaining a dynamic range and a signal-to-noise ratio of 1000 at a 1-ps time resolution. In practice, there is real noise in the system, which only exacerbates the problem. Sources of noise include the x rays which are not absorbed in a transmission mode photocathode and the high-energy primary photoelectrons which are not focusable. These can produce fluorescence and secondary electrons when they impinge on various electrodes. Ions produced by Coulomb collisions between the photoelectrons and the residual background gas in the tube can also cause problems,

especially at high current densities.

The largest source of noise for our streak cameras is the recording system, i.e., the image intensifier and the film. Inspired by work reported by Wiedwald and Lerche,[14] we characterized our Tri-X recording film for signal-to-noise ratio as shown in Fig. 3, with results similar to theirs. The films were scanned on a Perkin–Elmer PDS Microdensitometer with a 50×50-μm size aperture. The contribution to the S/N ratio by the electronics in the PDS is being studied. As expected, the S/N can be improved by increasing the pixel area, while sacrificing temporal and/or spatial resolution. When the image intensifier characteristics are included, the S/N ratio will degrade further. We are currently continuing work in this area. The alternative to film is CCD arrays, which are reported to be quantum noise limited for three orders of magnitude of intensity.[14]

In order to interpret the experimental data recorded with the streak cameras correctly, one needs to relate unambiguously the time of the x-ray emission to the incident laser pulse. To this end, optical fiducials are now routinely recorded on all of the x-ray streak cameras at LLE.[15]

II. TIME-RESOLVED X-RAY IMAGING

The diagnosis of the hydrodynamics of microfabricated targets irradiated by intense laser light is a central part of the investigation of laser fusion concepts. At LLE we use a 10-μm-diam pinhole coupled to an x-ray streak camera to follow the trajectory of the shell of the imploding targets in their own self-emission.[16] In the future we also hope to be able to follow the implosion in absorption, using x-ray backlighting techniques. To examine two-dimensional features in detail, it is vital to maintain accurate spatial registration of the x-ray image of the target on the photocathode slit. A pointing accuracy of $\pm$ 5 μm with respect to the geometric center of the original target position is required to image the final core, which may have a diameter <20 μm.

The x-ray imaging pinhole assembly for our instrument is mounted in a dichroic structure to permit visible alignment to $\pm$ 50 μm with a collimating telescope from the opposing port. The pinhole is laser drilled in a strip of Ta foil, 1.5 mm wide and 20 μm thick. This pinhole substrate is held between two glass washers 7 mm in diameter with a 0.5-mm center hole to pass the x rays. A beryllium foil blast shield which can be remotely positioned is used to protect the dichroic pinhole assembly from the target debris. The pinhole is positioned by a flexible coupling and fulcrum with two orthogonal motorized actuators, one along the spatial axis and the other along the temporal axis. The x-ray image is magnified by $15\times$ to the streak camera, where the final high-accuracy alignment is performed with a cross-slit photocathode. This cathode, which is illustrated in Fig. 4, incorporates a 1-mm-wide slot near one end for spatial alignment, in addition to the normal 100-μm time-resolving slit.

With the pinhole centered on the cross slit with the optical viewing system and the streak camera in focus mode, a low-power target shot is taken to measure the magnification and the misalignment. Figure 5 shows the contour of an image from a 327-μm-diam target. The circle inscribed through the four limb peaks of the image shows where the target is located. The two bisections of the circle parallel to the slit and slot images will give the mispointing of the system. In Fig. 5 the pinhole is seen to be positioned 18 μm high, above the temporal slit. The final pointing is a function of the measurement of the limb position and the number of iterations (shoot, measure, move pinhole). The pinhole-positioning actuators can be moved accurately to less than 5 μm and define the pointing accuracy. The pinhole is moved laterally to the center of the photocathode for streaked experiments, without changing cathodes. This system also permits simple checks to be made on the alignment periodically.

A further improvement to this system will be to isolate the streak camera from the vacuum chamber. This will permit the placement of an x-ray film pack on the cathode plate. A slot in the film is used to define the photocathode slit, allowing a streak record to be taken at arbitrary chords across the target, absolutely registered with the two-dimensional time-integrated x-ray image.

X-ray microscopes have demonstrated a 1-μm spatial resolution capability but not when coupled to any currently available streak cameras.[17] To match properly the spatial resolution of the streak camera, one needs to magnify the x-ray image $\sim50\times$, and then by another factor of 4 in the streak tube and coupling optics before being amplified by the image intensifier. Such an instrument would, of course, have a very restricted field of view. The x-ray flux from the target

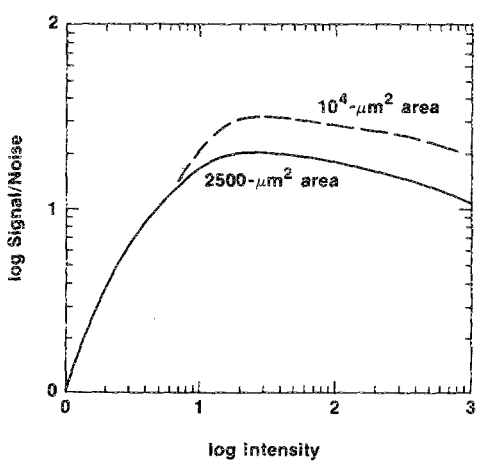

FIG. 3. Signal-to-noise characteristics for Tri-X film for two different pixel areas.

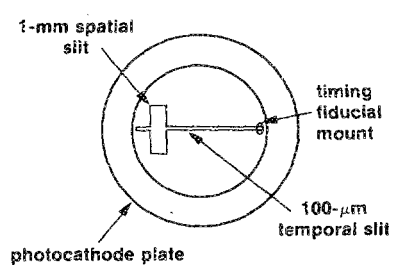

FIG. 4. Schematic of the cross-slit photocathode used for accurate spatial registration of the image.

becomes the limiting factor for achieving the 1-μm, 1-ps resolution goal with reasonable dynamic range.

III. REFLECTION MODE PHOTOCATHODE, SOFT-X-RAY STREAK CAMERA

An x-ray transmission grating coupled to an x-ray streak camera is an ideal instrument for broadband, time-resolved, soft-x-ray spectroscopy. These devices are versatile and easy to set up, and have been used extensively as a diagnostic for laser fusion[18–20] and x-ray laser experiments.[21] The main limitation of these instruments has been the long-wavelength cutoff of the spectral range by absorption due to the photocathode substrate. Practical limits are about 250 Å. There is a growing need to extend the wavelength region for time-resolved spectroscopy to softer x rays and throughout the VUV wavelength range. To this end, we have modified one of the large-format x-ray streak tubes at LLE to operate with a reflection mode photocathode[22] and incorporated it into a spectroscopic system which has a free-standing transmission grating as the dispersive element.[23] The long-wavelength detection limit of this instrument is now defined by the grating period and/or the work function of the photocathode material. It is fascinating to note that one of the first working x-ray streak tubes (reported in 1974) did operate with a reflection mode photocathode.[24]

Reflection mode photocathodes have some definite advantages over transmission mode photocathodes, especially for soft-x-ray detection. First, a reflection mode photocathode can be formed on any thick, robust, conductive substrate, eliminating the need for the fragile 1000-Å-thick cathode substrate. Second, front-surface photoemitters are more efficient since the photon energy is preferentially deposited where it is most effective, near the photocathode–vacuum interface. A further enhancement in the secondary electron quantum yield can be obtained with a reflection mode photocathode when it is operated with the photons incident at some grazing angle ϕ. In this case the normal component of the x-ray attenuation length is reduced by $\sin\phi$, which gives a better match between it and the electron escape depth.

The implementation of a reflection mode photocathode in a commercial x-ray streak tube is not practical, since all of them incorporate a mesh in close proximity to the cathode for the accelerating field. If one were to use such a tube and the photons were incident through the mesh, the secondary electrons and fluorescent x rays produced off the mesh would significantly reduce the signal-to-noise ratio and the spatial resolution. A second method, which uses the gap between the cathode and the mesh as the entrance aperture for the photons, would severely restrict the solid angle subtended by the cathode. Typically this interelectrode spacing is 1–2 mm.

The large-format x-ray streak tube, standard at LLE, incorporates a 2×60-mm slot aperture for the accelerating electrode rather than a mesh. This provides an ideal access window for implementing a reflection mode photocathode. The astigmatism introduced in the electron optics by this asymmetric aperture is corrected with a cylindrical focus lens at the anode. The slit cut into the side of the accelerating electrode and the MACOR insulators as shown in Fig. 6 is the x-ray access aperture. This slit is far from the tube axis and therefore introduces a negligible perturbation on the photoelectron trajectories. This aperture is 1 mm wide, defining the photocathode width, and 2 cm long, determining the solid angle subtended. The photons are incident on the cathode at a grazing angle of 30°; thus 40 mm of photocathode length are illuminated.

Figure 7 shows how this streak tube has been incorporated into a soft-x-ray, time-resolving, transmission grating spectrograph for OMEGA experiments. The maximum diffraction angle to which the streak tube can be moved is 20°, and defines the long-wavelength detection limit according to the grating equation,

$$m\lambda = d\sin\theta,$$

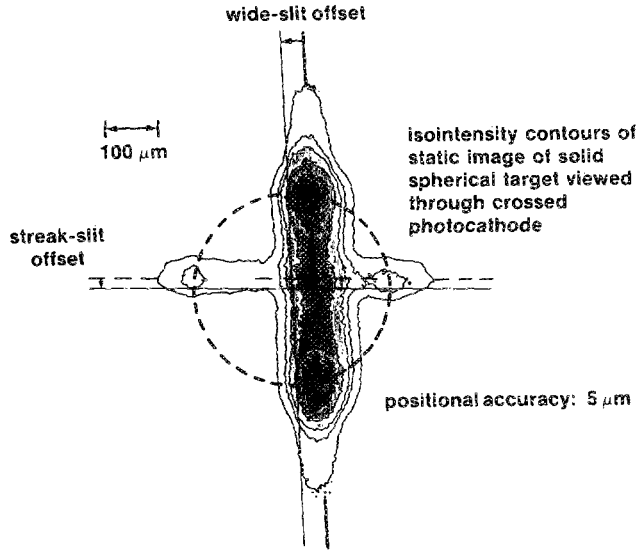

FIG. 5. Technique for registering the target image on the time-resolving slit.

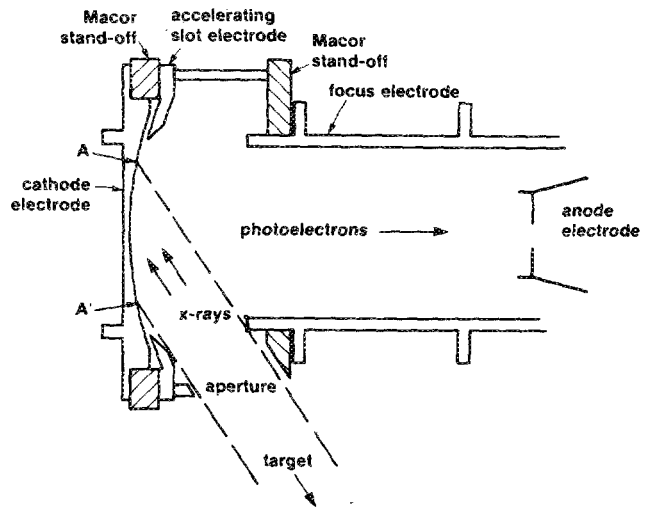

FIG. 6. Schematic of the streak tube front-end electrode configuration. The plane is through the long axis of the slot and shows the location of the x-ray access aperture.

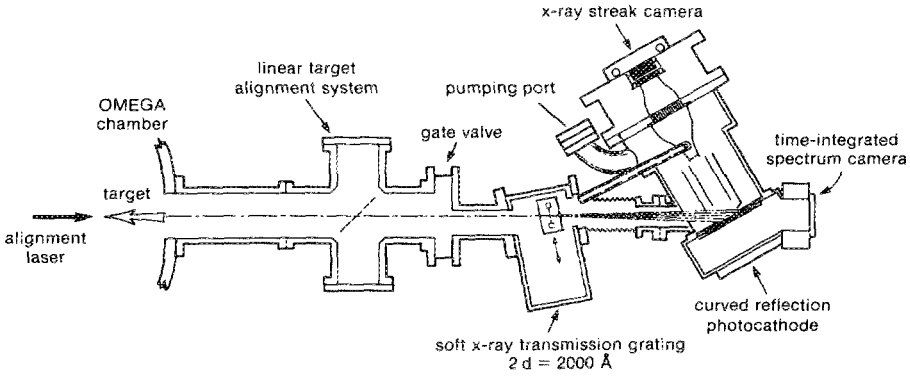

FIG. 7. Schematic of the soft-x-ray, reflection mode photocathode, transmission grating time-resolving spectrograph.

where m is the diffraction order, λ is the photon wavelength, d is the grating period, and θ is the diffraction angle. The spectral resolution of the instrument is a compromise between the source size (S) and the degree of collimation provided by the grating slit width (A):

$$\Delta\lambda = d\left(\frac{S+A}{L}+\frac{A}{D}\right),$$

where $L = 150$ cm is the source-to-grating distance and $D = 30$ to 90 cm is the grating-to-detector distance. With a 0.2-μm period grating we can achieve a spectral resolution of 0.5 Å.

ACKNOWLEDGMENT

This work was supported by the U.S. DOE Office of Inertial Fusion under agreement No. DE-FC08-85DP40200 and by the Laser Fusion Feasibility Project at the Laboratory for Laser Energetics, which has the following sponsors: Empire State Electric Energy Research Corporation, New York State Energy Research and Development Authority, Ontario Hydro, and the University of Rochester. Such support does not imply endorsement of the content of this article by any of the above parties.

[a] Present address: Optikos, 143 Albany Street, Cambridge, MA 02139.

[1] H. N. Kornblum and V. W. Silvinsky, Rev. Sci. Instrum. **49**, 1204 (1978); R. H. Day, in *Proceedings of the NATO Advanced Study Institute on High Density Plasma Diagnostics*, Pascali, Italy, 1983.
[2] D. R. Kania, P. Bell, and J. Trebes, SPIE J. **831**, 160 (1987); D. R. Kania (these proceedings).
[3] M. J. Eckart, R. L. Hanks, J. D. Kilkenny, R. Pasha, J. D. Wiedwald, and J. D. Hares, Rev. Sci. Instrum. **57**, 2046 (1986); J. D. Hares, SPIE J. **831**, 165 (1987); J. D. Kilkenny (these proceedings).
[4] For reviews of current developments on x-ray streak cameras, see *Proceedings of the 12–17th Congresses on High Speed Photography and Photonics* and *Proceedings on High Speed Photography, Videography, and Photonics III–V*, both published by SPIE, Bellingham, WA.
[5] R. L. Kauffman, G. Stradling, and H. Medecki, SPIE J. **348**, 752 (1984).
[6] M. C. Richardson, G. G. Gregory, S. A. Letzring, R. S. Marjoribanks, B. Yaakobi, B. L. Henke, P. A. Jaanimagi, and A. Hauer, SPIE J. **569**, 149 (1985).
[7] P. A. Jaanimagi and B. L. Henke, Bull. Am. Phys. Soc. **28**, 5U21 (1983).
[8] B. L. Henke, J. Knauer, and K. Premaratne, J. Appl. Phys. **52**, 1509 (1981).
[9] A. J. Lieber, H. D. Sutphin, C. B. Webb, and A. H. Williams, Electro-Opt. Syst. Des. (No. 9), 26 (1976); A. J. Lieber, SPIE J. **189**, 452 (1979).
[10] G. Mourou and W. Knox, Appl. Phys. Lett. **35**, 492 (1979).
[11] S. G. Glendinning and H. Medecki, Rev. Sci. Instrum. **57**, 2184 (1986); G. L. Stradling, SPIE J. **832**, 379 (1987).
[12] D. S. Montgomery, R. P. Drake, B. A. Jones, and J. D. Wiedwald, SPIE J. **832**, 283 (1987).
[13] ITT specifications for Generation II devices range from 10% to 40%.
[14] J. D. Wiedwald and R. A. Lerche, SPIE J. **832**, 275 (1987).
[15] P. A. Jaanimagi, L. DaSilva, G. G. Gregory, C. Hestdalen, C. D. Kiika, R. Kotmel, and M. C. Richardson, Rev. Sci. Instrum. **57**, 2189 (1986).
[16] G. G. Gregory, S. A. Letzring, M. C. Richardson, and C. D. Kiikka, SPIE J. **569**, 141 (1985); G. G. Gregory, P. A. Jaanimagi, P. W. McKenty, S. A. Letzring, and M. C. Richardson, SPIE J. **832**, 383 (1987).
[17] R. H. Price, in *Low Energy X-Ray Diagnostics*, AIP Conference Proceedings No. **75**, edited by D. T. Attwood and B. L. Henke (American Institute of Physics, New York, 1981), p. 189.
[18] N. M. Ceglio, in *Low Energy X-Ray Diagnostics*, AIP Conference Proceedings No. **75**, edited by D. T. Attwood and B. L. Henke (American Institute of Physics, New York, 1981), p. 210.
[19] N. M. Ceglio, M. Roth, and A. M. Hawryluk, in *Low Energy X-Ray Diagnostics*, AIP Conference Proceedings No. **75**, edited by D. T. Attwood and B. L. Henke (American Institute of Physics, New York, 1981), p. 290.
[20] M. C. Richardson, R. S. Marjoribanks, S. A. Letzring, J. M. Forsyth, and D. M. Villeneuve, IEEE J. Quantum Electron. **QE-19**, 1861 (1983).
[21] D. L. Matthews, P. L. Hagelstein, M. D. Rosen, M. J. Eckart, N. M. Ceglio, A. U. Hazi, H. Medecki, B. J. MacGowan, J. E. Trebes, B. L. Whitten, E. M. Campbell, C. W. Hatcher, A. M. Hawryluk, R. L. Kauffman, L. D. Pleasance, G. Rambach, J. H. Scofield, G. Stone, and T. A. Weaver, Phys. Rev. Lett. **54**, 110 (1985).
[22] P. A. Jaanimagi, G. G. Gregory, S. A. Letzring, R. S. Marjoribanks, and M. C. Richardson, SPIE J. **831**, 179 (1987).
[23] A. M. Hawryluk, N. M. Ceglio, R. H. Price, J. Mélngaillis, and H. I. Smith, in *Low Energy X-Ray Diagnostics*, AIP Conference Proceedings No. **75**, edited by D. T. Attwood and B. L. Henke (American Institute of Physics, New York, 1981), p. 286.
[24] P. R. Bird, D. J. Bradley, A. G. Roddie, W. Sibbett, M. H. Key, M. Lamb, and C. L. S. Lewis, in *Proceedings of the 11th International Congress on High Speed Photography and Photonics*, 1974, p. 118.